ICG-induced NIR fluorescence mapping in patients with head & neck tumors after the previous radiotherapy

Sophie Cortese, Erwan Kerrien, Ilya Yakavets, Rokia Meilender, Romina Mastronicola, Sophie Renard, Agnès Leroux, Lina Bezdetnaya, Gilles Dolivet

ICG-induced NIR fluorescence mapping in patients with head & neck tumors after the previous radiotherapy

Sophie Cortese[1], Erwan Kerrien[2], Ilya Yakavets[1,3], Rokia Meilender[1], Romina Mastronicola[1], Sophie Renard[1], Agnes Leroux[1,3], Lina Bezdetnaya[1,3], Gilles Dolivet[1,3].

Abstract

Background: The distinction between tumor and healthy tissues is complicated in the areas previously subjected to radiation therapy (RT). This is related to the fact that tissues can undergo delayed and irreversible deterioration such as inflammation, vascular alteration and fibrosis. The trials related to the fluorescence –guided surgery (FSG) in Head and Neck Squamous Cell Carcinoma (HNSCC) patients, previously subjected to RT, have not yet been reported. The present study addresses for the first time the possibilities of tumor near-infrared (NIR) imaging using Indocynaine Green (ICG) in irradiated areas.

Methods: Four patients with histologically confirmed HNSCC were included in this study. All included patients were previously treated with RT with at least 50 Gy. RT-radiation fields from original treatment fully encompassed the second tumor or recurrence. ICG was injected via cephalic vein 45 min before the images were captured using a NIR camera system Artemis. The images were also captured before ICG injection serving as background signal. The fluorescence intensity measurements were carried out using specially designed software.

Results: ICG fluorescence clearly demonstrated a significant difference in fluorescence intensity between healthy and tumor tissues in 2 of 4 patients. Histology post-resection analysis confirmed a complete tumor resection with safe surgical margins. No difference between tumor and surrounding healthy tissue was detected in patients with an epidermoid carcinoma developed from sclerohypertrophic lichen.

Conclusions: In our pilot study, we clearly established the feasibility of using NIR FGS with ICG to delineate tumor and healthy tissues in irradiated areas in infiltrating lichen-free tumors.

1 Institut de Cancérologie de Lorraine ICL, 6 avenue de Bourgogne, 54519 Vandoeuvre-lès-Nancy, France

2 Inria, Université de Lorraine, Loria, UMR7503, Vandœuvre-lès-Nancy, France

3 CRAN, CNRS, UMR 7039, Université de Lorraine, Vandœuvre-lès-Nancy, France

1. Introduction

Head and neck squamous cell carcinoma (HNSCC) is the sixth most common malignant tumor in the world. The management of these cancers requires multidisciplinary treatments, including surgery, radiotherapy, chemotherapy, or targeted molecular therapy. Nevertheless, the prognostic remains poor, with more than 300,000 deaths each year. Surgical resection remains the primary treatment for HNSCCs. Margin status is considered as a major prognostic factor for overall survival [1]. Unfortunately, nowadays, there is a lack of adequate and reliable intraoperative tools to discriminate in a real-time tumor and normal healthy tissue. Frozen section evaluation during operation is routinely used to determine surgical margins. However, this procedure is time and cost consuming and can be inaccurate.

Regarding these expectations, NIR fluorescence imaging with indocyanine green (ICG) got increasing attention and was already applied to improve surgical resection in some clinical cases [2–4]. ICG is a small molecule that has been clinically approved by the United States Food and Drug Administration (USFDA). After intravenous injection, ICG binds to serum proteins and behaves as a nanoparticle, rending possible its enrichment in tumor via the enhanced permeability and retention (EPR) effect [5]. The first application of ICG for fluorescence-guided surgery (FGS) for head and neck cancers was reported in 2012 in preclinical models [6]. Later on, ICG-FGS clinical trials were realized in 6 patients with parapharyngeal space tumors and appeared to be effective for the detection and resection of the parapharyngeal space tumors with preserving functions [4]. It worth noting that other imaging techniques such as Lugol chromoendoscopy, confocal endoscopy, autofluorescence imaging, or narrow-band imaging are mainly used to guide biopsies and to detect suspicious precancerous lesions. Whereas exogenous near-infrared induced fluorescence approach is much preferable in tumor resection and metastasis detection [7].

Compared with initial surgery, the distinction between tumor and healthy tissues is even more complicated in patients with previous radiotherapy (RT). Frequently from the clinical and radiobiological point of view, radionecrosis is hardly distinguishable from progressive relapse. This is related to the fact that tissues can undergo delayed and irreversible deteriorations such as inflammation, fibrosis, vascular alterations, and cellular depletion [8–11].

Until now, the trials related to FGS in head and neck (H&N) cancer patients previously subjected to RT have not been reported. The present study addresses for the

first time the feasibility of ICG-mediated FGS to delineate H&N tumors in the areas previously subjected to ionizing radiation, so-called irradiation territory. In a small sample of previously irradiated HNSCC patients, we demonstrated the possibility to visualize the tumor and discriminate it from normal tissue in the irradiated territory with ICG-based fluorescence. We also discuss the possible reasons of failure observed in some patients.

2. Materials and Methods

2.1. Patients

All patients were recruited between December 2017 and August 2018. Patients had biopsy-proven squamous cell carcinoma with an antecedent of HNSCC tumors treated by surgery with healthy margins followed by radiotherapy. **All patients received RT dose of 66Gy at the tumor site and 50Gy on the area of lymph nodes (Table 1).** RT-radiation areas fully encompass the second tumor or recurrence. **For Patient 1 the secondary tumor was located in the lymph node irradiation area. Dosimetry analysis in resection areas demonstrated that applied RT doses were 50Gy (patient 1), 60Gy/63Gy (patients 2 and 3), and 47Gy (patient 4).** Only two patients had an indication for chemotherapy, however, it was contraindicated due to the cardiovascular comorbidities. Intensity-Modulated Radiation Therapy (IMRT) was realized in 3 cases. One of them (patient 4) presented severe acute mucositis toxicity (grade 3) and late toxicity with dysphagia xerostomia (grade 3) along with neck fibrosis (grade 3). For patients 2 & 3, acute and late toxicity with moderate xerostomia and neck fibrosis (grade 2) were registered. Patient 1 received conventional radiotherapy. No significant treatment-related side-effects were noted for this patient.

Patients with metastatic disease, severe hepatic, and renal dysfunction were excluded from this study. The clinical trial was sponsored by the "*Institut de Cancérologie de Lorraine*" (Lorraine Cancer Center): clinicaltrials.gov identifier: NCT02920216, European Clinical Trials Database ID-RCB: 2016-A00014-47. It was approved by the French National Drug Agency (ANSM) and by the ethical committee (CPP Est III).

Characteristics of both previous and actual tumors, along with applied treatment modalities, are summarized in Table 1. **The patients were classified by pathological stage (pTNM) according to the 8th edition of the Union for International Cancer Control (UICC) classification [12].** All patients were originally treated with curative intention. For each patient, the therapeutic decision was validated in the interdisciplinary tumor board (ITB). All subjects gave their consent before being included in this study.

2.2. ICG administration

ICG (25 mg/vial; Indocyanine Green; Serb, Paris, France) was resuspended in 10 mL of the solvent provided by the manufacturer for the final concentration 2.5 mg/mL. The prepared ICG solution was administered at a dose 0.25mg/kg via the cephalic vein. The first fluorescence measurement was performed before ICG injection, right after clearing the tumor area in order to obtain a neutral background. The second fluorescence measurement was taken in the interval 30-45 min after ICG injection, before tumor excision. Compared to usual surgery, ICG-based procedure adds 20-30 min, mostly due to camera adjustment.

2.3. Imaging system

Fluorescent intraoperative imaging was performed using a near-infrared (NIR) camera system (Artemis, Quest Medical Imaging BV, The Netherlands). The Artemis is a high-definition, dual-band (white-light and NIR) camera system capable of concurrent NIR emission and detection while generating real-time video (Figure 1). For the surgical procedure, we used an excitation laser with peak intensity at 793 nm, and NIR signal was selected with a long-pass filter at 805 nm. The camera is supplied with the “Quest Spectrum Viewer” software (Quest Medical Imaging BV, The Netherlands), which allows viewing of recorded videos during and away from operations.

2.4. Software

The video sequences follow the QIFS proprietary Quest Imaging File System format, which encodes 3 images for each frame: one in the visible spectrum and two others in the near-infrared, one of which captures the ICG-induced fluorescence with peak emission at 805 nm. This latter image was used in our study to compute the statistics on the fluorescent signal in the regions of interest (ROI). The ROIs were delineated in the color image in the visible spectrum. The supplied software does not allow a simple longitudinal analysis of the data. As a consequence, we developed custom software consisting of two parts. First, each image sequence is stabilized using a non-rigid registration algorithm [13] in order to compensate for small motions induced by the manual holding of the retractors. Secondly, a Graphical User Interface, called “QIFSViewer” was developed, based on the open-source cross-platform PoLAR library [14]. Besides image sequence visualization functionalities (interactive image browsing, zooming, panning, and window/level adjustment), the software enables a switch between color and fluorescence images, manual delineation of ROIs with any desired shape and computation of statistical analysis on each ROI. Due to prior image stabilization, ROIs only have to be delineated on one image and remain

consistent for the whole sequence. The statistics are provided for each ROI and each image as the mean, median, standard deviation and area, and saved under the Comma-Separated Values (CSV, Excel compliant) format.

2.5. Histopathology

Tumor and extemporaneous frozen section biopsies were further analyzed by the histopathology department. Based on hematoxylin-eosin (H&E) staining, the frozen section biopsies were classified as positive (+) or negative (-). In the case of a positive result, a margin-widening operation was planned.

2.6. Statistics

The mean fluorescence intensity of ROI was calculated subsequently for each frame, averaged in time at least 150 frames, and presented as mean ± standard deviation (SD) for each image sequence.

3. Results

3.1. Clinical study

Four patients were included in this study. Patients and tumor characteristics are detailed in Table 1. The average patients' age was 71 years old (56-84). All primary tumors (Panel A, Figs. 2-5) were treated with surgery and adjuvant RT. Dosimetry treating fields in sagittal (left or right), axial (down), and coronal (front) views are presented in Panel B of Figures 2-5. The delay between primary and secondary tumors varied between 3 and 9 years. Two of four patients developed secondary SCC tumors at the site different from initial ones (patients 1 and 2). The third patient had a recurrence. Patient 4 presented a second tumor developed near the previous surgically treated site but after a five years delay, making the hypothesis of a local recurrence unlikely. All secondary tumors were completely surgically excised with safe margins. The final histopathological assessment demonstrated invasive SCC in 3 patients (Cases 1, 2, and 4), while the patient 3 had a tumor *in situ*.

3.2. Fluorescence Imaging Analysis

All patients we imaged intraoperatively using ARTEMIS camera. To quantify the fluorescence intensities in ROIs, we developed custom software. First of all, the software enables the stabilization of the video sequences using a non-rigid registration algorithm in order to compensate for small motions induced by the manual holding of the retractors. Secondly, the software performs statistical analysis on each ROI, which could be manually

delineated in both brightfield and fluorescence image sequences making possible the quantitative analysis of the video.

For patients 1 and 2, the tumor displayed bright fluorescence emission that clearly contrasted with surrounding normal tissue (Fig. 2, C-H; Fig. 3, C-H). Based on these images, the histograms were plotted displaying the fluorescent intensity of the tumor and surrounding healthy tissue before and after ICG injections (Figs. 2&3, I). The tumor/surrounding normal tissue ratios varied from 1.5 (Case 1) to 2 (Case 2), thus clearly indicating ICG selectivity for tumor tissue.

The tumor characteristics for the last two patients (Cases 3&4) were complicated by the presence of lichen (Figs. 4&5). In these patients, already the primary SCC tumors were developed on the bed of lichen. Lichen is acknowledged as chronic inflammatory mucosae, which in some cases can be transformed into malignant tumor [15].

For patient 3, visual intraoperative observations evidenced some contrast between tumor and surrounding normal tissue (Fig. 4, C-H). However, the quantitative fluorescence imaging analysis demonstrated a similar signal in three examined areas: normal, tumor, and lichen (Fig. 4, I). Thus, no selectivity was detectable between cancerous lesions and normal tissue.

As for the fourth patient, we did not observe any difference between tumor and other tissues, neither visually nor by fluorescence analysis (Fig. 5, C-I).

3.3. Anatomopathologic diagnosis

Anatomopathologic diagnosis of the tumors is presented in Table 2. Histologically tumors of the first two patients (Patients 1&2) were infiltrating **squamous cell carcinomas** with approximately 20 mm in diameter. Tumors in two other patients were different from previous ones. In Patient 3 histological analysis demonstrated large central ulceration with **squamous cell carcinoma** *in situ* associated with extensive sclero-hypertrophic lichen. The last patient (Patient 4) had infiltrating differentiated squamous cell carcinoma with a lichen lesion. The tumor size in these patients was 15-17 mm.

4. Discussion

Treatment with concomitant chemoradiotherapy has emerged as a gold standard in the majority of advanced squamous cell carcinoma of the head and neck. Nevertheless, the prognosis of these cancers remains poor, with a high rate of recurrences [16]. Salvage surgery thus becomes the only therapeutic alternative for the patient with recurrent HNSCC offering better tumor control and survival [17]. Still, surgery for patients with recurrent HNSCC is challenging and remains associated with high morbidity and poor

oncological outcomes. Also, not all patients are suitable candidates for salvage surgery, and an accurate selection of these patients is a major issue.

It should be noted that positive margins after salvage surgery are of the order 18-22% [18], and several studies have demonstrated the negative impact of positive margins after salvage surgery on survival [19–23]. The detection of resection margins is mainly based on visualization, palpation, and surgeon's experience. Several groups started investigating intraoperative NIR imaging with ICG to distinguish between normal and malignant tissue tumors in head and neck cancer and demonstrated a good imaging contrast [4,24,25]. There is always concern that previous radical irradiation would damage the capillary and microvasculature network, provoking necrosis at the tumor site, tissue remodeling, and as such changes in optical tissue properties, hindering access of molecules to the tumor and making difficult clinical perception of tumor limits [26]. In patients with recurrent nasopharyngeal carcinoma after previous radiotherapy ICG-based fluorescence mapping of sentinel lymph nodes was already reported [27] and demonstrated an accurate nodal staging. The trials addressing ICG-mediated mapping in H&N cancer patients after irradiation have not been performed. The purpose of the current study was to inspect the feasibility of using ICG intraoperative fluorescence imaging to differentiate tumors from normal tissues in patients with recurrent head and neck tumors after radical radiotherapy. In fact, salvage surgeries in H&N cancer patients are challenging procedures, with associated morbidity, considerably reduced functional integrity, and poor prognosis. There are several criteria for Patients' stratification for salvage surgery suitability [28]. However, for most patients, salvage surgery is contraindicated, and the only limited number of H&N cancer patients could be offered salvage surgery after radical RT. Thus, only four HNSCC patients could be selected for our study.

Previous irradiations commonly provoke an increased rate of wound healing complications in salvage surgery [29,30]. Several predisposition risk factors have been reported for poor wound healing, such as glucose level, smoking, nutrition, and alcohol abuse [31]. Therefore, the selection of patients and preoperative planning is recommended to optimize outcomes and avoid complications. A rigorous surgical technique, the use of a pedicled or free flap, post-operative local wound care, and peri-opérative antibiotics allows to reduce post-operative complications. In our case, 2 patients were ancient smokers and alcohol dependant (patients 1&2), while two others had no risk factors. In all four patients, we did not notice major wound healing issues.

In patient 3 we could detect visually ICG-induced fluorescence at the tumor site, however fluorescence image analysis did not show any contrast with surrounding healthy

tissue or lichen mass. It is recognized that open-field optical imaging varies in function of different external conditions (camera position, over-head or ceiling lamps…) and, therefore, a pertinent rigorous analysis that would consider all variables is hardly possible. As was accurately proposed by Keulen and co-workers [24], a "surgical view" rather than true quantitative analysis should be considered. From this point of view, a "surgical view" in patient 3 met our expectations related to tumor delineation. Visually the contrast in this patient was less pronounced compared with that in Patients 1&2. One of the hypotheses could be that a weak fluorescence is related to extensive sclerohypertrophic lichen, thus rending difficult ICG diffusion across the tumor. The same holds for patient 4, where the fluorescence signal was undetectable in a "surgical view" and this lack of contrast was further confirmed by fluorescence analysis. **It worth noting that Patients 1 and 4 had a lower irradiation dose in the resection areas compared with two other patients**. **However, the contrast of ICG staining was largely in favor of Patient 1. Therefore, it seems difficult to establish the impact of RT dose in the resection area on the contrast of ICG staining.**

5. Conclusion

Our pilot study on ICG–induced NIR fluorescence mapping in HNSCC patients previously subjected to radical radiotherapy clearly established the feasibility of using this technique to delimitate free of lichen tumors. To support the "surgical view" with the quantitative statistical analysis, the custom software was developed. According to the data obtained, the presence of thick necrotic area or old lichen lesions seems to be a major limitation for efficient NIR mapping. The final confirmation warrants investigation in a bigger patient sample. Difficulties in including patients after radical radiotherapy are related to the fact that only limited numbers of patients are eligible for salvage surgery.

Overall, NIR fluorescence-guided surgery represents an invaluable tool for tumor detection and resection because of the real-time feedback and the contrast that it offers. Our ongoing study addresses optimal conditions (ICG concentration, the time interval between ICG injection, and fluorescence measurements) for ICG-FGS in previously irradiated tumor areas.

Funding: This research was funded by the Institut de Cancérologie de Lorraine.

References

[1] T.A. Iseli, M.J. Lin, A. Tsui, A. Guiney, D. Wiesenfeld, C.E. Iseli, Are wider surgical margins needed for early oral tongue cancer?, J. Laryngol. Otol. 126 (2012) 289–294. https://doi.org/10.1017/S002221511100332X.

[2] F.P.R. Verbeek, J.R. van der Vorst, B.E. Schaafsma, M. Hutteman, B.A. Bonsing, F.W.B. van Leeuwen, J.V. Frangioni, C.J.H. van de Velde, R.-J. Swijnenburg, A.L. Vahrmeijer, Image-guided hepatopancreatobiliary surgery using near-infrared fluorescent light, J. Hepato-Biliary-Pancreat. Sci. 19 (2012) 626–637. https://doi.org/10.1007/s00534-012-0534-6.

[3] J.R. van der Vorst, B.E. Schaafsma, M. Hutteman, F.P.R. Verbeek, G.-J. Liefers, H.H. Hartgrink, V.T.H.B.M. Smit, C.W.G.M. Löwik, C.J.H. van de Velde, J.V. Frangioni, A.L. Vahrmeijer, Near-infrared fluorescence-guided resection of colorectal liver metastases, Cancer. 119 (2013) 3411–3418. https://doi.org/10.1002/cncr.28203.

[4] J. Yokoyama, S. Ooba, M. Fujimaki, T. Anzai, R. Yoshii, M. Kojima, K. Ikeda, Impact of indocyanine green fluorescent image-guided surgery for parapharyngeal space tumours, J. Cranio-Maxillo-Fac. Surg. Off. Publ. Eur. Assoc. Cranio-Maxillo-Fac. Surg. 42 (2014) 835–838. https://doi.org/10.1016/j.jcms.2013.12.001.

[5] C. Egloff-Juras, L. Bezdetnaya, G. Dolivet, H.-P. Lassalle, NIR fluorescence-guided tumor surgery: new strategies for the use of indocyanine green, Int. J. Nanomedicine. 14 (2019) 7823–7838. https://doi.org/10.2147/IJN.S207486.

[6] M. Fujimaki, J. Yokoyama, S. Ohba, T. Anzai, Y. Yoshii, S. Ito, M. Kojima, K. Ikeda, Dynamic imaging in determining the optimum surgical time for NIR fluorescent image-guided surgery - a preliminary study., Head Neck Oncol. 4 (2012) 50.

[7] I. Atallah, C. Milet, J.-L. Coll, E. Reyt, C.A. Righini, A. Hurbin, Role of near-infrared fluorescence imaging in head and neck cancer surgery: from animal models to humans, Eur. Arch. Otorhinolaryngol. 272 (2015) 2593–2600. https://doi.org/10.1007/s00405-014-3224-y.

[8] P. Gallet, B. Phulpin, J.-L. Merlin, A. Leroux, P. Bravetti, H. Mecellem, N. Tran, G. Dolivet, Long-Term Alterations of Cytokines and Growth Factors Expression in Irradiated Tissues and Relation with Histological Severity Scoring, PLoS ONE. 6 (2011). https://doi.org/10.1371/journal.pone.0029399.

[9] R.P. Hill, H.-P. Rodemann, J.H. Hendry, S.A. Roberts, M.S. Anscher, Normal tissue radiobiology: from the laboratory to the clinic, Int. J. Radiat. Oncol. • Biol. • Phys. 49 (2001) 353–365. https://doi.org/10.1016/S0360-3016(00)01484-X.

[10] J. Williams, Y. Chen, P. Rubin, J. Finkelstein, P. Okunieff, The biological basis of a comprehensive grading system for the adverse effects of cancer treatment, Semin. Radiat. Oncol. 13 (2003) 182–188. https://doi.org/10.1016/S1053-4296(03)00045-6.

[11] H.B. Stone, C.N. Coleman, M.S. Anscher, W.H. McBride, Effects of radiation on normal tissue: consequences and mechanisms, Lancet Oncol. 4 (2003) 529–536. https://doi.org/10.1016/S1470-2045(03)01191-4.

[12] J.D. Brierley, M.K. Gospodarowicz, Witterkind, TNM Classification of Malignant Tumours, 8th Edition, Wiley-Blackwell, 2017. https://www.wiley.com/en-us/TNM+Classification+of+Malignant+Tumours%2C+8th+Edition-p-9781119263579 (accessed April 30, 2020).

[13] M.P. Heinrich, M. Jenkinson, M. Bhushan, T. Matin, F.V. Gleeson, S.M. Brady, J.A. Schnabel, MIND: Modality independent neighbourhood descriptor for multi-modal deformable registration, Med. Image Anal. 16 (2012) 1423–1435. https://doi.org/10.1016/j.media.2012.05.008.

[14] P.-J. Petitprez, E. Kerrien, P.-F. Villard, PoLAR: A Portable Library for Augmented Reality, in: 2016 IEEE Int. Symp. Mix. Augment. Real. ISMAR-Adjun., 2016: pp. 227–230. https://doi.org/10.1109/ISMAR-Adjunct.2016.0081.

[15] S. Saraf, N. Ghanee, The Malignant Transformation of Oral Lichen Planus and Oral Lichenoid Lesions, a Case Report and Review of the Literature, J. Clin. Anat. Pathol. 1 (2019) 1.
[16] J.P. Pignon, J. Bourhis, C. Domenge, L. Designé, Chemotherapy added to locoregional treatment for head and neck squamous-cell carcinoma: three meta-analyses of updated individual data. MACH-NC Collaborative Group. Meta-Analysis of Chemotherapy on Head and Neck Cancer, Lancet Lond. Engl. 355 (2000) 949–955.
[17] T. Maruo, S. Zenda, T. Shinozaki, T. Tomioka, W. Okano, M. Sakuraba, M. Tahara, R. Hayashi, Comparison of salvage surgery for recurrent or residual head and neck squamous cell carcinoma, Jpn. J. Clin. Oncol. (2019). https://doi.org/10.1093/jjco/hyz176.
[18] I.B. Tan, G. Dolivet, P. Ceruse, V.V. Poorten, G. Roest, W. Rauschning, Temoporfin-mediated photodynamic therapy in patients with advanced, incurable head and neck cancer: A multicenter study, Head Neck. 32 (2010) 1597–1604. https://doi.org/10.1002/hed.21368.
[19] A.S. Jones, Z. Bin Hanafi, V. Nadapalan, N.J. Roland, A. Kinsella, T.R. Helliwell, Do positive resection margins after ablative surgery for head and neck cancer adversely affect prognosis? A study of 352 patients with recurrent carcinoma following radiotherapy treated by salvage surgery, Br. J. Cancer. 74 (1996) 128–132. https://doi.org/10.1038/bjc.1996.327.
[20] M. Hamoir, E. Holvoet, J. Ambroise, B. Lengelé, S. Schmitz, Salvage surgery in recurrent head and neck squamous cell carcinoma: Oncologic outcome and predictors of disease free survival, Oral Oncol. 67 (2017) 1–9. https://doi.org/10.1016/j.oraloncology.2017.01.008.
[21] G.J. Schwartz, R.H. Mehta, B.L. Wenig, C. Shaligram, L.G. Portugal, Salvage treatment for recurrent squamous cell carcinoma of the oral cavity, Head Neck. 22 (2000) 34–41. https://doi.org/10.1002/(sici)1097-0347(200001)22:1<34::aid-hed6>3.0.co;2-3.
[22] L.P. Kowalski, Results of salvage treatment of the neck in patients with oral cancer, Arch. Otolaryngol. Head Neck Surg. 128 (2002) 58–62. https://doi.org/10.1001/archotol.128.1.58.
[23] B.S. Koo, Y.C. Lim, J.S. Lee, E.C. Choi, Recurrence and salvage treatment of squamous cell carcinoma of the oral cavity, Oral Oncol. 42 (2006) 789–794. https://doi.org/10.1016/j.oraloncology.2005.11.016.
[24] S. van Keulen, N. Nishio, S. Fakurnejad, N.S. van den Berg, G. Lu, A. Birkeland, B.A. Martin, T. Forouzanfar, A.D. Colevas, E.L. Rosenthal, Intraoperative Tumor Assessment Using Real-Time Molecular Imaging in Head and Neck Cancer Patients, J. Am. Coll. Surg. 229 (2019) 560-567.e1. https://doi.org/10.1016/j.jamcollsurg.2019.09.007.
[25] Y. Wang, D. Xie, Z. Wang, X. Zhang, Q. Zhang, Y. Wang, A.D. Newton, S. Singhal, H. Cai, Y. Wang, Q. Lu, Q. Hu, Z. Wang, Kinetics of indocyanine green: Optimizing tumor to normal tissue fluorescence in image-guided oral cancer surgery applications, Head Neck. 41 (2019) 1032–1038. https://doi.org/10.1002/hed.25541.
[26] C. Jaillet, W. Morelle, M.-C. Slomianny, V. Paget, G. Tarlet, V. Buard, S. Selbonne, F. Caffin, E. Rannou, P. Martinez, A. François, F. Foulquier, F. Allain, F. Milliat, O. Guipaud, Radiation-induced changes in the glycome of endothelial cells with functional consequences, Sci. Rep. 7 (2017) 1–16. https://doi.org/10.1038/s41598-017-05563-y.
[27] J.Y.W. Chan, R.K.Y. Tsang, S.T.S. Wong, W.I. Wei, Indocyanine green fluorescence mapping of sentinel lymph node in patients with recurrent nasopharyngeal carcinoma

after previous radiotherapy, Head Neck. 37 (2015) E169-173. https://doi.org/10.1002/hed.24052.
[28] H.K. Tan, R. Giger, A. Auperin, J. Bourhis, F. Janot, S. Temam, Salvage surgery after concomitant chemoradiation in head and neck squamous cell carcinomas - stratification for postsalvage survival, Head Neck. 32 (2010) 139–147. https://doi.org/10.1002/hed.21159.
[29] C.-A. Righini, K. Nadour, C. Faure, R. Rtail, N. Morel, V. Beneyton, E. Reyt, Salvage surgery after radiotherapy for oropharyngeal cancer. Treatment complications and oncological results, Eur. Ann. Otorhinolaryngol. Head Neck Dis. 129 (2012) 11–16. https://doi.org/10.1016/j.anorl.2011.06.002.
[30] M. Hamoir, S. Schmitz, C. Suarez, P. Strojan, K.A. Hutcheson, J.P. Rodrigo, W.M. Mendenhall, R. Simo, N.F. Saba, A.K. D'Cruz, M. Haigentz, C.R. Bradford, E.M. Genden, A. Rinaldo, A. Ferlito, The Current Role of Salvage Surgery in Recurrent Head and Neck Squamous Cell Carcinoma, Cancers. 10 (2018) 267. https://doi.org/10.3390/cancers10080267.
[31] S.R. Schwartz, B. Yueh, C. Maynard, J. Daley, W. Henderson, S.F. Khuri, Predictors of wound complications after laryngectomy: A study of over 2000 patients, Otolaryngol.--Head Neck Surg. Off. J. Am. Acad. Otolaryngol.-Head Neck Surg. 131 (2004) 61–68. https://doi.org/10.1016/j.otohns.2003.08.028.

Table 1. Patients and tumor characteristics

Case	**1**	**2**	**3**	**4**
Previous tumor site	Oral cavity Left tongue/Floor of mouth	Larynx (Epiglottis)	Oral cavity **(Cheek mucosae).**	Oral cavity **(Right maxillary tuberosity)**
Treatment of previous tumor	Surgery/ radiotherapy Conventional (T:66 Gy/N:50Gy)	Surgery/ radiotherapy IMRT (T:66 Gy/N:66Gy)	Surgery/ radiotherapy IMRT (T:66 Gy/N:66Gy)	Surgery/ radiotherapy IMRT (T: 66 Gy/N:50Gy)
Classification	pT2N1M0	pT2N2bM0	pT4N1M0	pT4N0M0
Secondary tumor site	Left threefold region	**Right** posterior pharyngeal wall	Recurrence	Right **oral mucosae** hard palate-
Delay preceding secondary tumor (years)	9	4	3	5
Type of tumor resection	Partial pharyngo-laryngectomy	Posterior pharyngectomy	Mucosal resection	Mucosal resection
Classification	pT2	pT2	pTis	pT1

Table 2. Anatomopathologic analysis of the second tumors

Case	Anatomopathologic analysis of the tumor
1	**Squamous cell carcinoma** moderately differentiated, poorly mature, infiltrating. Tumor size: 20 mm. Intraepithelial neoplasia lesions on the periphery of the tumor at a distance from resection margins.
2	Inflitrating well-differentiated squamous cell carcinoma. Tumor size was 25 mm and 6 mm thickness. Central tumor ulcerated on the surface. Inflammatory stroma. Tumor was distant from resection margins.
3	**Squamous cell carcinoma** in situ around the ulceration, associated with more extensive of sclero- hypertrophic lichen. Tumor size: 10 × 15 mm. Presence of large ulceration. No invasive carcinomatous structure.
4	Hard palate: fragment of 4.5 × 4 × 0.5 cm. Poorly defined and altered tumor area about 1.5 cm in diameter. Infiltrating differentiated **squamous cell carcinoma** associated with lichen lesion.

Figures.

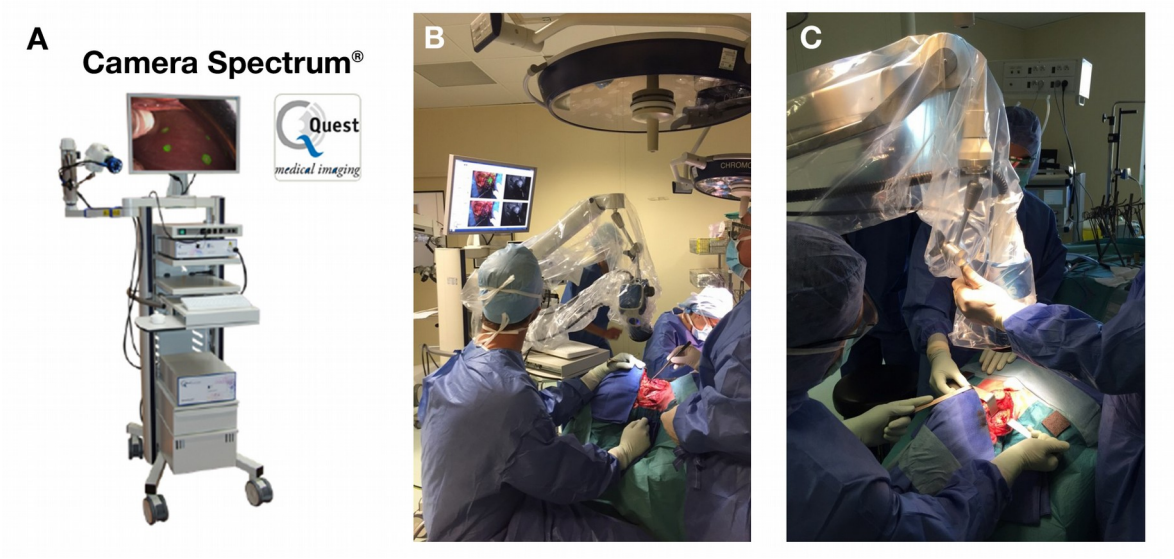

Fig. 1. Workflow for in situ fluorescence imaging. (A) Artemis NIR fluorescence imaging platform. (B&C) Examples of surgical operation using intraoperative fluorescence imaging for visualization of tumor margins using ICG.

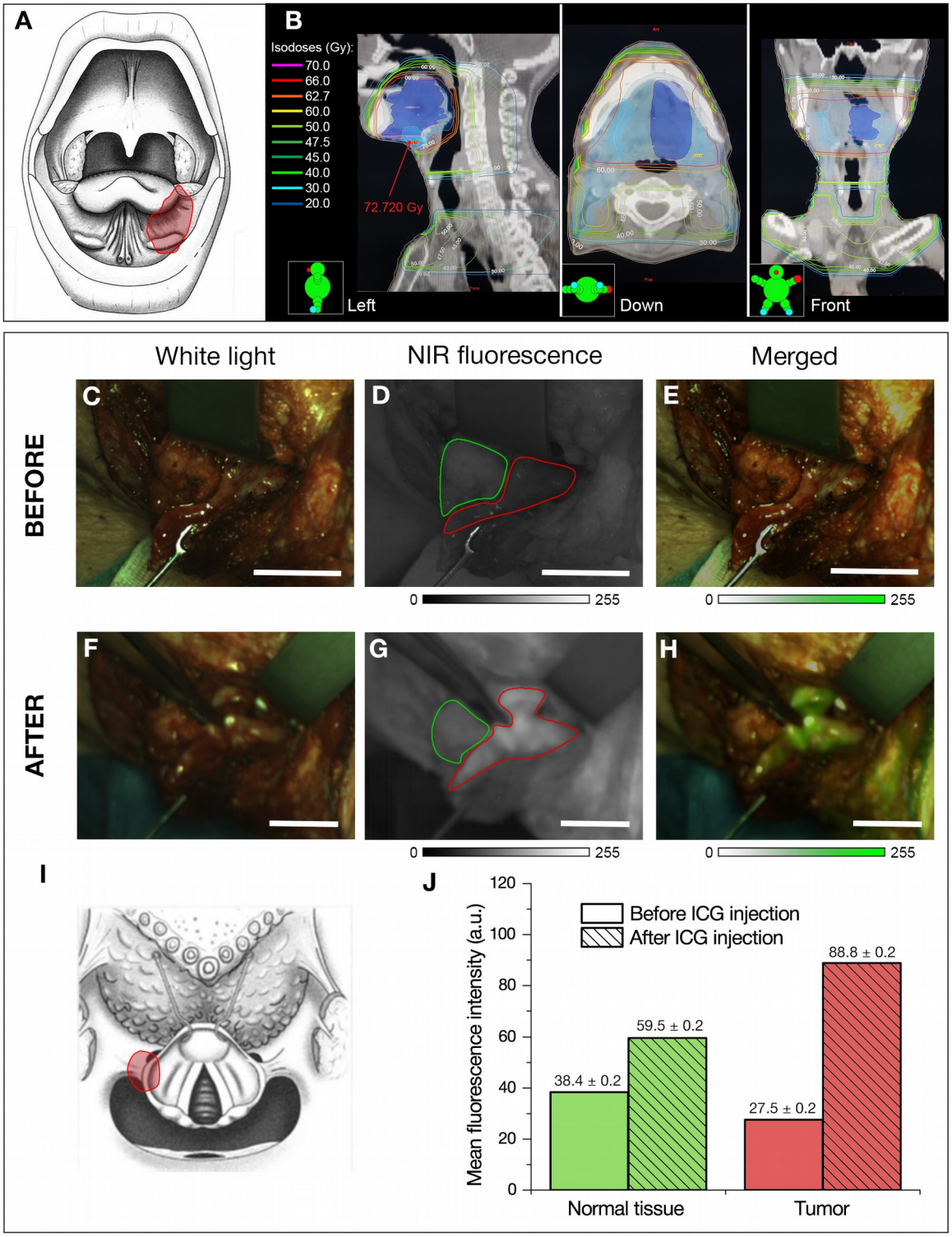

Fig. 2. Case 1. Patient with left threefold region tumor. (A) Schema representing the location and extension of the first tumor and (B) RT dosimetry. Intraoperative imaging: (C, F) white light images; (D, G) *in situ* NIR fluorescence images and (E, H) merged images. Tumor area is highlighted in red. The reference (normal tissue) is represented by a green contour. Scale bar 2 cm. **(I) Schema representing the location and extension of the second tumor (red contour).** (J) The histogram of the mean fluorescence intensity in the areas corresponding to the normal tissue and tumor before and after ICG injection. The data are presented as mean ± SD.

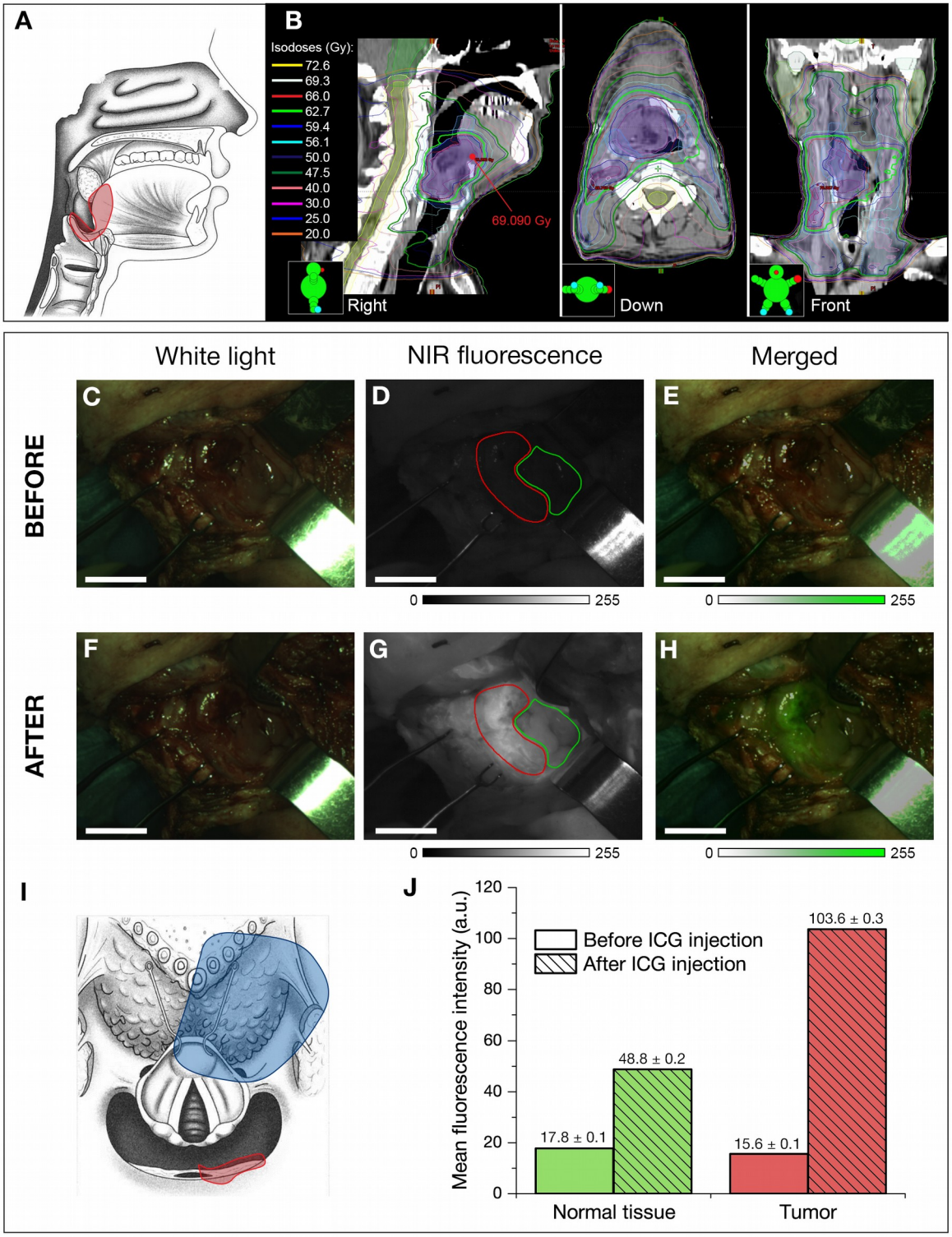

Fig. 3. Case 2. Patient with **right** posterior pharyngeal wall tumor. (A) Schema representing the location and extension of the first tumor and (B) RT dosimetry. Intraoperative imaging: (C, F) white light images; (D, G) *in situ* NIR fluorescence images and (E, H) merged images. Tumor area is highlighted in red. The reference (normal tissue) is represented by a green contour. Scale bar 2 cm. **(I) Schema representing the location and extension of the second tumor (red contour) compared to the first one (blue contour).** (J) The histogram of the mean fluorescence intensity in the areas corresponding to normal tissue and tumor before and after ICG injection. The data are presented as mean ± SD.

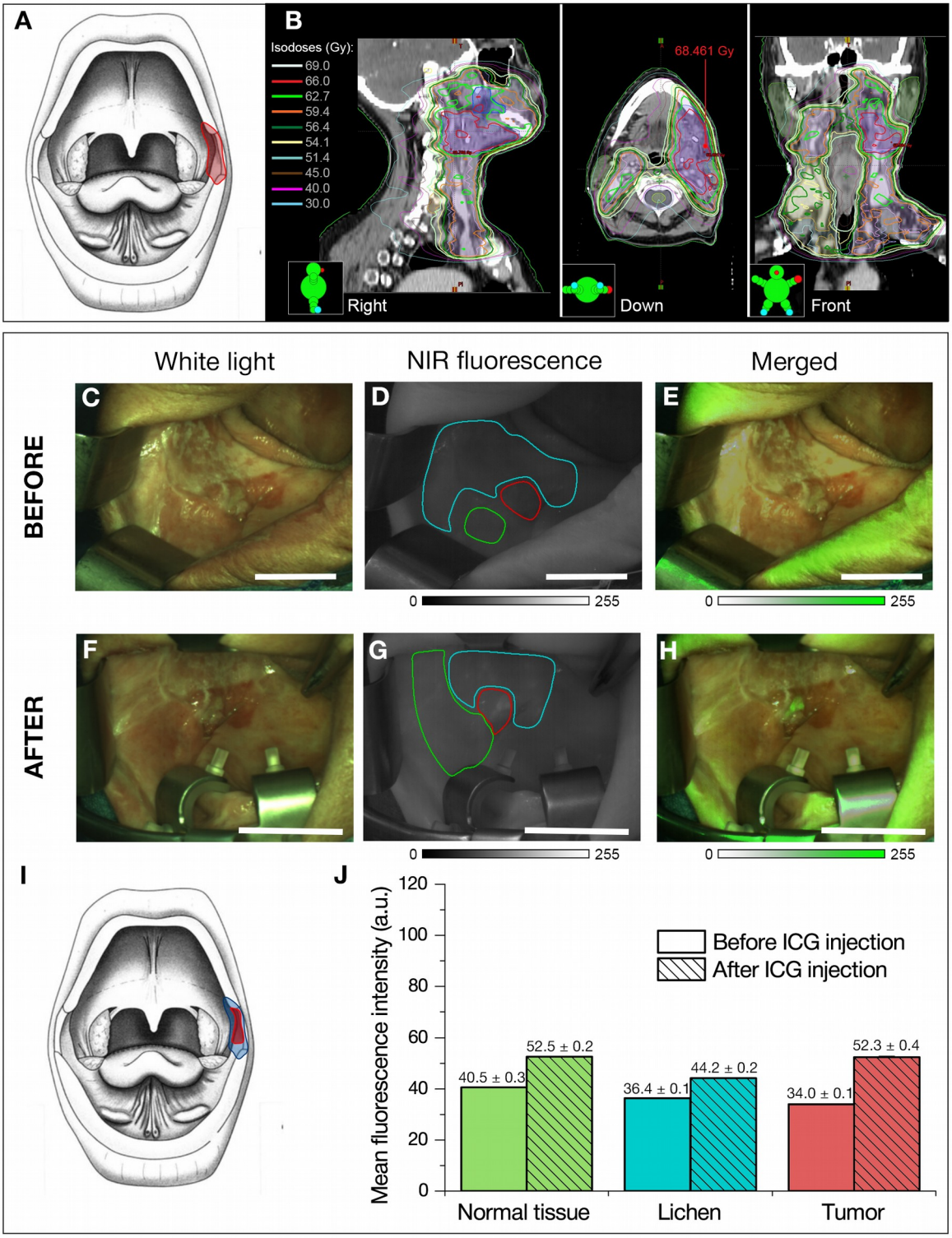

Fig. 4. Case 3. Patient with left **mucosae c**heek tumor. (A) Schema representing the location and extension of the first tumor and (B) RT dosimetry. Intraoperative imaging: (C, F) white light images; (D, G) *in situ* NIR fluorescence images and (E, H) merged images. Tumor and lichen areas are highlighted in red and cyan, respectively. The reference (normal tissue) is represented by a green contour. Scale bar – 2 cm. **(I) Schema representing the location and extension of the second tumor (red contour) compared to the first one (blue contour).** (J) The histogram of mean fluorescence intensity in the areas corresponding to the normal tissue, lichen, and tumor before and after ICG injection. The data are presented as mean ± SD.

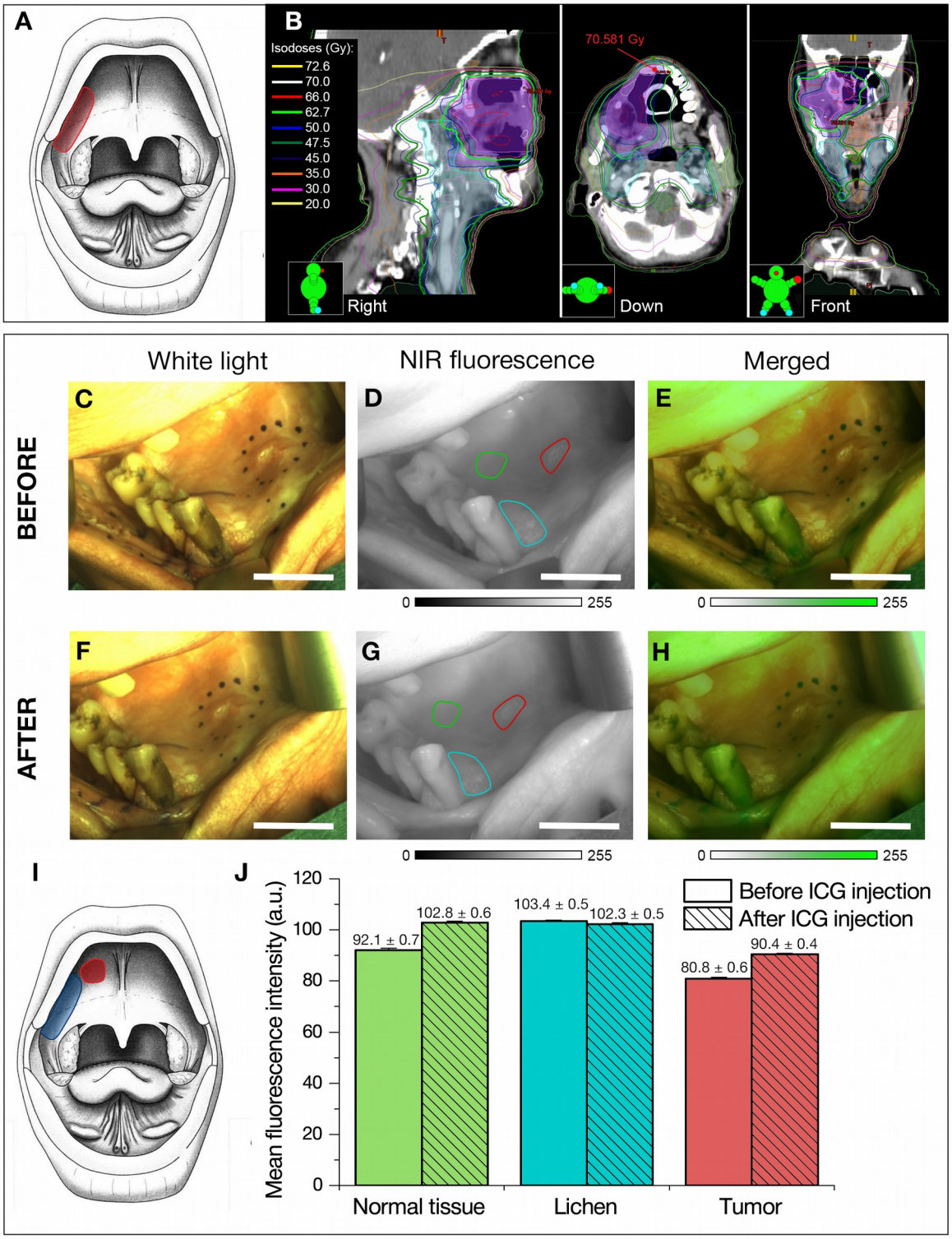

Fig. 5. Case 4. Patient with right **mucosae** hard palate tumor. (A) Schema representing the location and extension of the first tumor and (B) RT dosimetry. Intraoperative imaging: (C, F) white light images; (D, G) *in situ* NIR fluorescence images and (E, H) merged images. Tumor and lichen areas are highlighted in red and cyan, respectively. The reference (normal tissue) is represented by a green contour. Scale bar 2 cm. **(I) Schema representing the location and extension of the second tumor (red contour) compared to the first one (blue contour)**. (J) The histogram of mean fluorescence intensity in the areas corresponding to the normal tissue, lichen, and tumor before and after ICG injection. The data are presented as mean ± SD.